Geochemistry Geophysics Geosystems G3

Published by AGU and the Geochemical Society

Article
Volume 12, Number 12
28 December 2011
Q12018, doi:10.1029/2011GC003877
ISSN: 1525-2027

Dynamics of subduction initiation with different evolutionary pathways

Wei Leng and Michael Gurnis

Seismological Laboratory, California Institute of Technology, MS 252-21, Pasadena, California 91125, USA (leng@caltech.edu)

[1] Changes of plate motion may have induced subduction initiation (SI), but the tectonic history of SI is different from one subduction zone to another. Izu-Bonin-Mariana (IBM) SI, accompanied by strong backarc spreading and voluminous eruption of Boninites, contrasts with the Aleutians which shows neither. Using finite element models, we explore visco-elasto-plastic parameters and driving boundary conditions for SI evolution. With an imposed velocity, we find three different evolutionary modes of SI: continuous without backarc spreading, continuous with backarc spreading and a segmented mode. With an increase in the coefficient of friction and a decrease in the rate of plastic weakening, the amount of convergence needed for SI increases from ~20 to ~220 km, while the mode changes from segmented to continuous with backarc spreading and eventually to continuous without backarc spreading. If the imposed velocity boundary condition is replaced with an imposed stress, the amount of convergence needed for SI is reduced and backarc spreading does not occur. These geodynamic models provide a basis for understanding the divergent geological pathways of SI. First, IBM evolution is consistent with subduction of an old strong plate with an imposed velocity which founders causing intense backarc spreading and Boninitic volcanism. Second, the New Hebrides SI is in the segmented mode due to its weak plate strength. Third, the Puysegur SI is in the continuous without backarc spreading mode with no associated volcanic activities. Fourth, the Aleutians SI has neither trench rollback nor backarc spreading because the slab is regulated by constant ridge-push forces.

Components: 8700 words, 10 figures, 3 tables.

Keywords: backarc spreading; evolutionary pathways; subduction initiation.

Index Terms: 0545 Computational Geophysics: Modeling (1952, 4255, 4316); 3060 Marine Geology and Geophysics: Subduction zone processes (1031, 3613, 8170, 8413); 8034 Structural Geology: Rheology and friction of fault zones (8163).

Received 16 September 2011; **Revised** 11 November 2011; **Accepted** 11 November 2011; **Published** 28 December 2011.

Leng, W., and M. Gurnis (2011), Dynamics of subduction initiation with different evolutionary pathways, *Geochem. Geophys. Geosyst.*, *12*, Q12018, doi:10.1029/2011GC003877.

1. Introduction

[2] New subduction zones initiate as plate motions evolve, but the mechanics of the process remain obscure. Despite such limitations, significant progress has been made on our understanding of the nucleation of subduction from a combination of approaches, including geological synthesis [*Stern and Bloomer*, 1992; *Niu et al.*, 2003; *Gurnis et al.*, 2004; *Stern*, 2004; *Sutherland et al.*, 2010], detailed studies of volcanic and sedimentary rock sequences of specific nucleating margins [*House et al.*, 2002;

Sutherland et al., 2009; *Reagan et al.*, 2010], and geodynamic models [*McKenzie*, 1977; *Mueller and Phillips*, 1991; *Toth and Gurnis*, 1998; *Hall et al.*, 2003; *Gurnis et al.*, 2004; *Nikolaeva et al.*, 2010]. Generally, two major conceptual models have been proposed to explain subduction initiation (SI): spontaneous and forced (or induced) [*Gurnis et al.*, 2004; *Stern*, 2004].

[3] In the spontaneous subduction initiation model, the formation of a new subduction zone is driven solely by the density contrast between adjacent plates. The density difference arises from either the thermal effects of different plate ages or from a difference of chemical composition (or crustal thickness) between the two plates which span the boundary [e.g., *Niu et al.*, 2003]. Passive margins along old continents have the largest density contrast and could be the preferred tectonic setting for spontaneous initiation [*Cloetingh et al.*, 1989]. Subduction initiation may spontaneously occur at passive margins given a potentially large chemical density contrast and small ductile strength of the subcontinental lithospheric mantle [*Nikolaeva et al.*, 2010]. However, there are two difficulties for the spontaneous subduction initiation model. First, the forces resisting subduction initiation (including plate bending and friction on the fault plane) for old plates are large [*McKenzie*, 1977; *Cloetingh et al.*, 1989; *Mueller and Phillips*, 1991]. Specifically, continuous plate aging does not provide a more favorable condition for subduction initiation during passive margin evolution because plate strength increases more rapidly than buoyancy as the oceanic lithosphere ages [*Cloetingh et al.*, 1989]. How the resisting forces can be overcome during subduction initiation remains unclear. Second, there are no obvious Cenozoic examples of subduction initiation at passive margins [*Stern*, 2004], despite the fact that nearly half of all subduction zones that exist today nucleated during the Cenozoic [*Gurnis et al.*, 2004].

[4] Alternatively, initiation can be facilitated by external forces which is called induced subduction initiation [*Toth and Gurnis*, 1998; *Hall et al.*, 2003; *Gurnis et al.*, 2004; *Stern*, 2004]. Under continuous compression from a force external to the immediate vicinity of the nucleating margin, a relatively old plate can underthrust a young plate. The negative buoyancy of the old plate eventually exceeds the resistant forces after about 100 km of convergence [*McKenzie*, 1977; *Toth and Gurnis*, 1998; *Hall et al.*, 2003; *Gurnis et al.*, 2004]. Under some circumstances, subduction initiation can catastrophically unfold as characterized by the rapid descent of the old plate within the upper mantle with a corresponding rapid ascent of asthenospheric materials beneath the young, overriding plate. The descent of the old plate leads to backarc spreading consistent with the voluminous eruption of Boninites during the formation of the Izu-Bonin-Mariana (IBM) subduction zone [*Stern and Bloomer*, 1992]. A prediction of the induced model is that subduction initiation should generally follow changes of plate motion, especially after strong compression along relatively weak margins (such as transform faults or extinct spreading centers). For example, since the middle Miocene, subduction initiation has been occurring along the northern segment of the Macquarie Ridge Complex south of New Zealand following the progressive changes in the relative motion between the Australian and Pacific plates [*Sutherland et al.*, 2000].

[5] Although the induced model compares favorably to the geological record, substantial questions remain. First, *Hall et al.* [2003] and *Gurnis et al.* [2004] observed catastrophic subduction initiation in their computational models only when using a small coefficient of friction, which may imply that large pore pressure plays a substantial role in reducing rock strength. It is important to study how subduction initiation evolves with large coefficients of friction which are more consistent with the results from rock friction experiments without large pore pressure [*Byerlee*, 1978]. Second, model results show that catastrophic subduction initiation is accompanied by strong backarc spreading and voluminous volcanism [*Hall et al.*, 2003; *Gurnis et al.*, 2004]. However, subduction initiation was not always accompanied by backarc extension. Some subduction zones that have nucleated since 50 Ma were not accompanied by backarc spreading or voluminous volcanism (e.g., the Aleutian subduction zone). Consequently, it is essential that we develop a fuller understanding of the mechanics of subduction initiation and the range of tectonic styles that can unfold during initiation.

[6] Here we explore the effects of mechanical parameters of the lithosphere and mantle on the evolutionary mode by which a new subduction zone forms. We first describe the geodynamic model we use for the numerical computations of induced subduction initiation. Then, we present a detailed analysis of the mechanics and accompanying tectonic evolution of subduction initiation as a function of plastic parameters, subducting plate age, and mechanical boundary conditions. We finish

Table 1. Model Constants

Symbols and Definition	Values
ρ_0 reference mantle density	3200 kg m^{-3}
α coefficient of thermal expansion	3×10^{-5} K^{-1}
g gravitational acceleration	9.8 m s^{-2}
C_p specific heat capacity	1000 J (kgK)$^{-1}$
G shear modulus	30 GPa
η_0 reference viscosity	5×10^{19} Pa s
$\dot{\varepsilon}_0$ reference strain rate	10^{-15} s^{-1}
n strain exponent	3.05
E activation energy	540 kJ mol^{-1}
R gas constant	8.31 J mol^{-1}
T_0 reference temperature	1400°C
η_{max} maximum viscosity	10^{25} Pa s
η_{min} minimum viscosity	10^{19} Pa s
C_f minimum cohesion	4.4 MPa

through a discussion of the models, their limitations, and their application to the geological record.

2. Geodynamic Model for Induced Subduction Initiation

[7] We use the finite element method to study the visco-elasto-plastic behavior of lithosphere and mantle material during induced subduction initiation in 2-D. The Ellipsis software [*Moresi et al.*, 2003] used here solves for the conservation equations of mass, momentum and energy. The approach has many similarities to that used in the Citcom mantle convection software [*Moresi et al.*, 1996] upon which Ellipsis was written. In contrast to the Eulerian scheme used in Citcom, Ellipsis uses Lagrangian particles for the accurate tracking of material properties and deformation history. The particles are advected with the flow field and the element stiffness matrix is assembled from integration over these particles; for computational details, see *Moresi et al.* [2003]. Here we only provide an overview of the visco-elasto-plastic formulation used for the subduction initiation models.

[8] The visco-elasticity of the material is described by an incompressible Maxwell material which assumes that the deformation rate is the sum of an elastic part and a viscous part:

$$\dot{\varepsilon}_{ij} = \frac{1}{2G}\dot{s}_{ij} + \frac{1}{2\eta}s_{ij}, \tag{1}$$

where $\dot{\varepsilon}_{ij}$, $\dot{s}_{ij}$, s_{ij}, G, and η are the strain rate, time rate of change of deviatoric stress, deviatoric stress, shear modulus and viscosity; i and j are spatial indices.

[9] The viscosity is non-Newtonian and temperature-dependent [*Karato and Wu*, 1993]:

$$\eta = \eta_0 \left(\frac{\dot{\varepsilon}_{II}}{\dot{\varepsilon}_0}\right)^{\left(\frac{1}{n}-1\right)} \exp\left[\frac{E}{nR}\left(\frac{1}{T}-\frac{1}{T_0}\right)\right], \tag{2}$$

where η_0, $\dot{\varepsilon}_{II}$, $\dot{\varepsilon}_0$, n, E, R, T, and T_0 are the reference viscosity, the second invariant of the deviatoric strain rate tensor, reference strain rate, strain exponent, activation energy, gas constant, and absolute and reference temperatures (both in Kelvin) (Table 1). In addition, the maximum and minimum viscosity are limited with η_{max} and η_{min}, respectively (Table 1).

[10] The plasticity of the material is enforced by a yield stress using the Drucker-Prager yield model:

$$\tau_y = \mu P + C, \tag{3}$$

where τ_y, μ, P and C are the yield stress, coefficient of friction, pressure and cohesion. Cohesion is the strength of the material at zero normal stress. We consider that mantle material becomes weaker as plastic strain increases [*Buck and Poliakov*, 1998; *Poliakov and Buck*, 1998]. This is modeled by linearly reducing μ and C with accumulated plastic strain as

$$\mu = \mu_0\left[1 - \min\left(1, \frac{\varepsilon_p}{\varepsilon_f}\right)\right], \tag{4}$$

$$C = C_f + (C_0 - C_f)\left[1 - \min\left(1, \frac{\varepsilon_p}{\varepsilon_f}\right)\right], \tag{5}$$

where μ_0, ε_p, ε_f, C_0, and C_f are the initial coefficient of friction, accumulated plastic strain, reference plastic strain, initial cohesion and minimum cohesion. In these two equations, "min" represents a function for getting a minimum value. ε_p represents the total accumulated plastic strain after the yield stress is reached. ε_f represents a threshold value of plastic strain. When accumulated plastic strain is larger than ε_f, no further weakening occurs. Table 1 shows the invariant model parameters used. We use a nominal initial cohesion C_0 = 44 MPa in our model.

[11] The nominal dimensions of the model domain are 1050 km in width by 350 km in depth (Figure 1a). The dimensions are later varied to test the sensitivity to domain size. The lithosphere is overlain by what is informally referred to as a "sticky air layer" (a compressible layer, 50 km in thickness), to simulate a free surface which has been proposed to be critical for producing single-

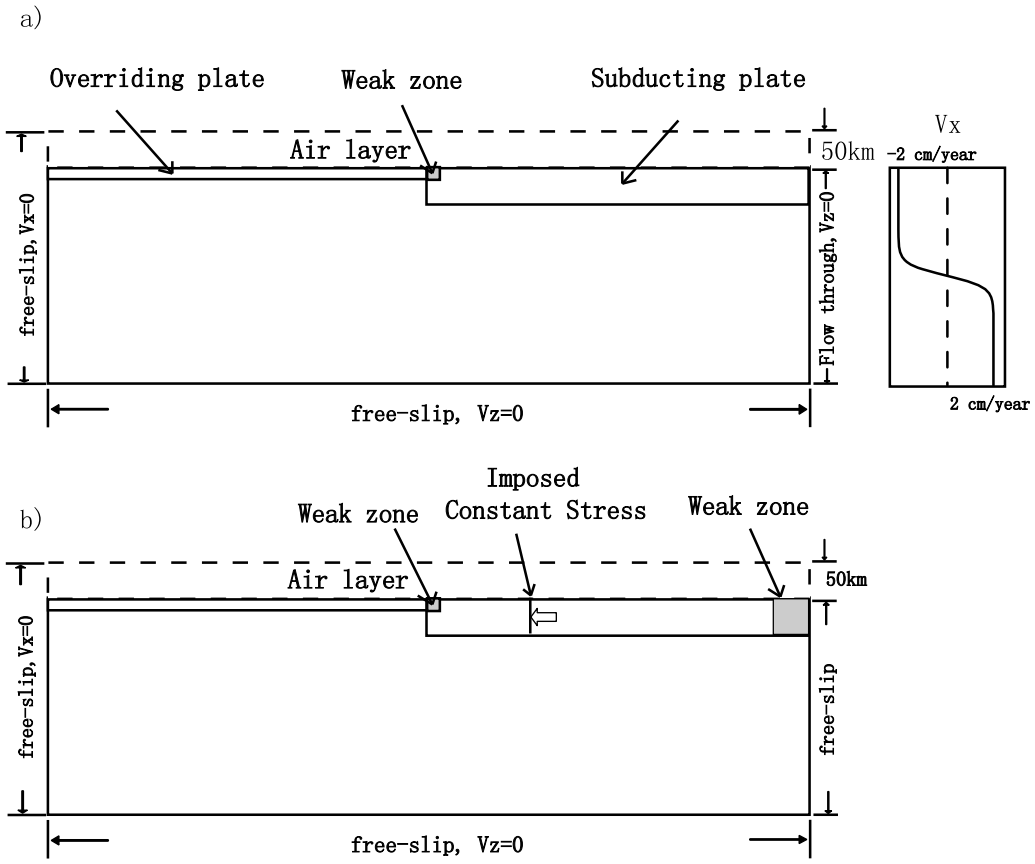

Figure 1. Computational model setup for induced subduction initiation. (a) Convergence is driven with an imposed constant velocity at the right boundary. To the right of the cross-section, the horizontal velocity (V_x) imposed at the right boundary of the box is shown. (b) Convergence is driven with an imposed constant stress in the plate. The constant stress is applied along a line on the old plate 700 km from the left boundary, down to a depth of 50 km.

sided subduction [*Crameri et al.*, 2011] (Figure 1a). The air layer has zero density with viscosity η_{min}. We use 128 × 64 elements with a nominal resolution of 8.2 km and 5.5 km in the horizontal and vertical directions, respectively. In each 8.2 km × 5.5 km element, we have 16 particles for tracking the material properties and strain history, which are initially uniformly distributed in the element and advected with the velocity field. The integration over an element is performed using the particles which exist in the element at any instant in time [*Moresi et al.*, 2003]. Therefore in terms of tracking the material properties and deformation history, the tracking accuracy is substantially higher than implied by an Eulerian scheme with the same number of elements with Gaussian quadrature [*Hughes*, 2000].

[12] The subducting and overriding plates, divided at the box center, have the same material properties except that their lithospheric ages are different (nominal values are 42 Ma *vs*. 2 Ma). A weak zone (17.5 by 17.5 km) is placed at the interface between the plates (Figure 1a). The top and bottom boundaries are isothermal and fixed at 0°C and the reference temperature T_0 = 1400°C, respectively. The left and right boundaries are thermally insulated. The initial temperature profiles for the mantle are computed using a half-space cooling model [*Turcotte and Schubert*, 2002]. The left, top and bottom boundaries are free-slip with no materials flowing in or out of the box. The vertical velocities at the right boundary are fixed at 0. With an imposed velocity boundary condition, we impose a horizontal velocity profile from the right side to push the old plate at a nominal velocity of 2 cm/year (Figure 1a). That is, the horizontal velocity is −2 cm/year from plate surface to 100 km depth (excluding the air layer), and 2 cm/year from 200 km to 300 km depth (Figure 1a); In the middle part from 100 km to 200 km depth, the horizontal velocity varies from −2 cm/year to 2 cm/year through a tanh() function. This profile satisfies the mass conservation for the lithosphere and the mantle. The imposed velocity

Table 2. Cases With Different Plasticity Parameters and Resulted Modes of Subduction Initiation[a]

Case	μ_0	ε_f	t_i (Myrs)	t_b (Myrs)	Modes
SI01	0.0	0.05	0.6	0.3	S
SI02	0.0	0.1	0.9	0.3	S
SI03	0.0	0.2	1.3	-	S
SI04	0.0	0.5	2.1	-	S
SI11	0.1	0.05	2.9	0.1	S
SI12	0.1	0.1	3.8	0.1	S
SI13	0.1	0.2	4.6	0.3	S
SI14	0.1	0.5	6.0	0.6	S
SI21	0.2	0.05	3.9	0.2	S
SI22	0.2	0.1	4.5	0.5	S
SI23	0.2	0.2	5.3	-	S
SI24	0.2	0.3	6.4	-	S
SI25	0.2	0.4	7.0	2.1	CB
SI26	0.2	0.5	8.0	1.7	CB
SI26h	0.2	0.5	7.9	1.5	CB
SI31	0.3	0.2	7.0	2.3	S
SI32	0.3	0.3	7.4	-	S
SI33	0.3	0.4	8.3	1.8	CB
SI41	0.4	0.2	6.6	3.9	S
SI42	0.4	0.3	7.7	4.3	CB
SI43	0.4	0.4	8.9	2.9	CB
SI51	0.5	0.5	9.8	-	C
SI61	0.6	0.05	5.3	2.3	S
SI62	0.6	0.1	6.0	3.2	S
SI63	0.6	0.2	8.5	5.4	CB
SI64	0.6	0.4	10.0	-	C
SI65	0.6	0.5	11.3	-	C

[a]Here μ_0 and ε_f are initial coefficient of friction and reference plastic strain. The initiation time, t_i, is defined as the time when the vertical velocity of the sampling point becomes larger than the imposed velocity at the right boundary. The backarc spreading time, t_b, is defined as the time interval between t_i and the time when backarc spreading starts. In the "mode" column, "S" represents the segmented initiation mode; "CB" represents the continuous initiation with backarc spreading mode; "C" represents the continuous initiation without backarc spreading mode.

boundary condition is appropriate either if the subduction initiation is induced within a small area along the strike of the boundaries of a large plate due to a change of its motion or if the forces on the plate are controlled from the far field. There is another possibility that the subduction initiation is induced by an imposed constant stress within the plate [e.g., *Toth and Gurnis*, 1998]. Conceptually, this constant stress boundary condition would mean that subduction initiation is driven by an invariant stress which, specifically, could arise from the ridge push force. We also test the effects of this kind of boundary condition on the mode of subduction initiation (Figure 1b). The right boundary is set to be free-slip for the imposed stress boundary condition. A nominal constant stress of 80 MPa, later varied between 60 and 120 MPa, is placed on the old plate 700 km from the left boundary, and applied on the top 50 km of the plate (Figure 1b). The position of the imposed stress does not move relative to the left boundary with time. We add another weak zone of 50 by 50 km at the right end of the old plate to detach the plate from the right boundary (Figure 1b).

3. Divergent Structural Modes of Subduction Initiation

3.1. Role of Plasticity

[13] We find that with an imposed velocity boundary condition, two plastic parameters, the initial coefficient of friction μ_0 and reference plastic strain ε_f, essentially determine the evolutionary mode (or pathway) of subduction initiation as shown with 26 cases where μ_0 is varied between 0.0 and 0.6 and ε_f is varied between 0.05 and 0.5 (Table 2). Generally, these cases can be categorized into one of three different evolutionary modes after several million years (Myrs) of convergence: continuous initiation with backarc spreading, continuous initiation without backarc spreading and a segmented subduction mode. We describe the characteristic features of each mode below.

[14] We start with a case (SI26) with a medium value of $\mu_0 = 0.2$ and a relatively large $\varepsilon_f = 0.5$, which gives rise to the mode of continuous initiation with backarc spreading. The cohesion reduces from the initial value to its minimum within 50% of accumulated plastic strain (equation (5)). After only 50 thousand years (Kyrs), a small dipping shear zone with concentrated strain rates starts to develop at the plate boundary (Figure 2). The velocity of the subducting slab only slowly increases for the first several Myrs of convergence (Figures 3a and 3d). After converging for ~8.0 Myrs, there is a rapid increase in the vertical velocity of the subducting slab marking the rapid bending of the old plate and the beginning of subduction initiation (Figures 3b and 3e). The velocity continues to increase and the descent of the plate leads to strong upwelling of asthenospheric materials beneath the overriding plate and above the subducting plate. The foundering of the subducting slab causes a strong traction on the overriding plate which eventually yields and leads to trench rollback and backarc spreading (Figures 3c and 3f). During the backarc spreading stage, the upwelling velocity of the asthenosphere above the descending plate can be as large as tens of cm/year (Figure 3c).

[15] We define that subduction initiation occurs when the vertical velocity of the subducting plate exceeds the imposed velocity. We monitor the

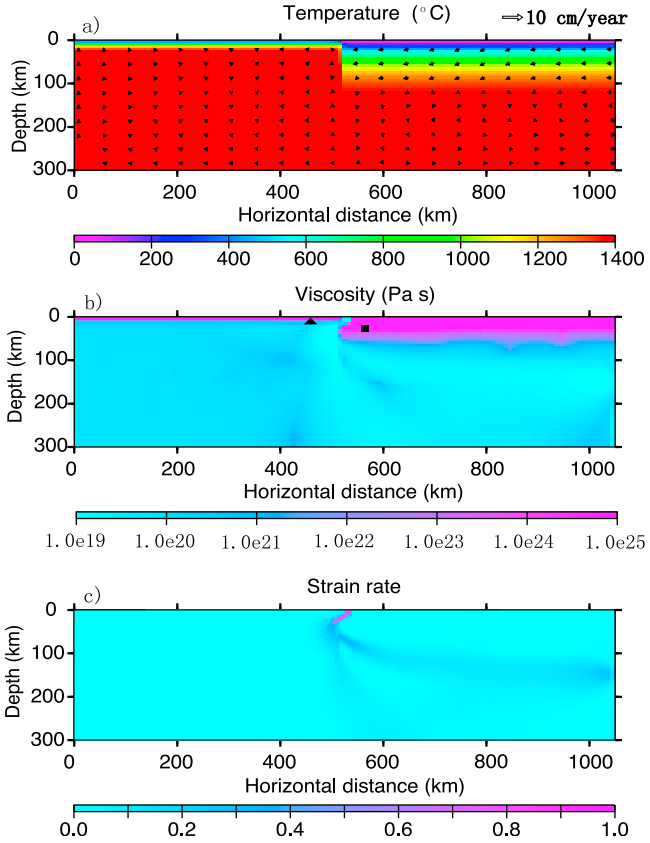

Figure 2. The (a) temperature, (b) viscosity, and (c) normalized strain rate of the initial state for case SI26 at 50 Kyrs. In Figure 2a, temperature is overlain by velocity vectors. In Figure 2b, a small black square and a triangle show the initial positions of the sampling points in the subducting plate and in the overriding plate, respectively. In Figure 2c, the strain rate is normalized by the maximum strain rate at this time, 9.7e-14 s^{-1}.

vertical velocity of the subducting plate at a sampling point which moves with the plate (black squares in Figures 2b and 3). A subduction initiation time, t_i, is defined as the time when the vertical velocity of the sampling point first becomes larger than the enforced plate velocity (2 cm/year). For case SI26, t_i = 8.0 Myrs (Figure 4a). We also monitor the horizontal velocity of the overriding plate during this process with another sampling point (black triangle in Figures 2b and 3). Due to the strong traction from the foundering of the subducting plate after subduction initiates, the horizontal velocity in the forearc region of the overriding plate starts to increase from ~0 to ~10 cm/year within a couple of Myrs after the initiation of subduction (Figure 4a). This eventually leads to backarc spreading at ~9.7 Myrs which is accompanied by an additional pulse of vertical velocity of the subducting plate (Figure 4a). The backarc spreading starts when the overriding plate completely yields and breaks at one point such that asthenospheric material reaches the surface. We define a backarc spreading time, t_b, as the time interval between t_i and the start of backarc spreading. For this case, t_b = 1.7 Myrs. Following the rapid descent of the plate and strong backarc spreading, the vertical velocity of the subducting plate slows as the plate approaches the bottom boundary, and the rate of backarc spreading decreases (Figure 4a).

[16] When μ_0 and ε_f are reduced to 0.1 and 0.2 (case SI13 in Table 2), respectively, compared to 0.2 and 0.5 in the prior model, we find a different evolutionary mode which we call a segmented initiation mode. Due to the decreased yield stress and reference plastic strain, the plate is initially weaker and the material weakens faster compared to the prior case, therefore subduction initiation occurs earlier (t_i = 4.6 Myrs, Figure 4b). Similar to the earlier case, the negative buoyancy bends the old plate but the vertical velocity of the subducting plate increases faster and earlier (after ~4.6 Myrs of convergence) (Figure 4b). However, in contrast to the continuous initiation mode, the descending

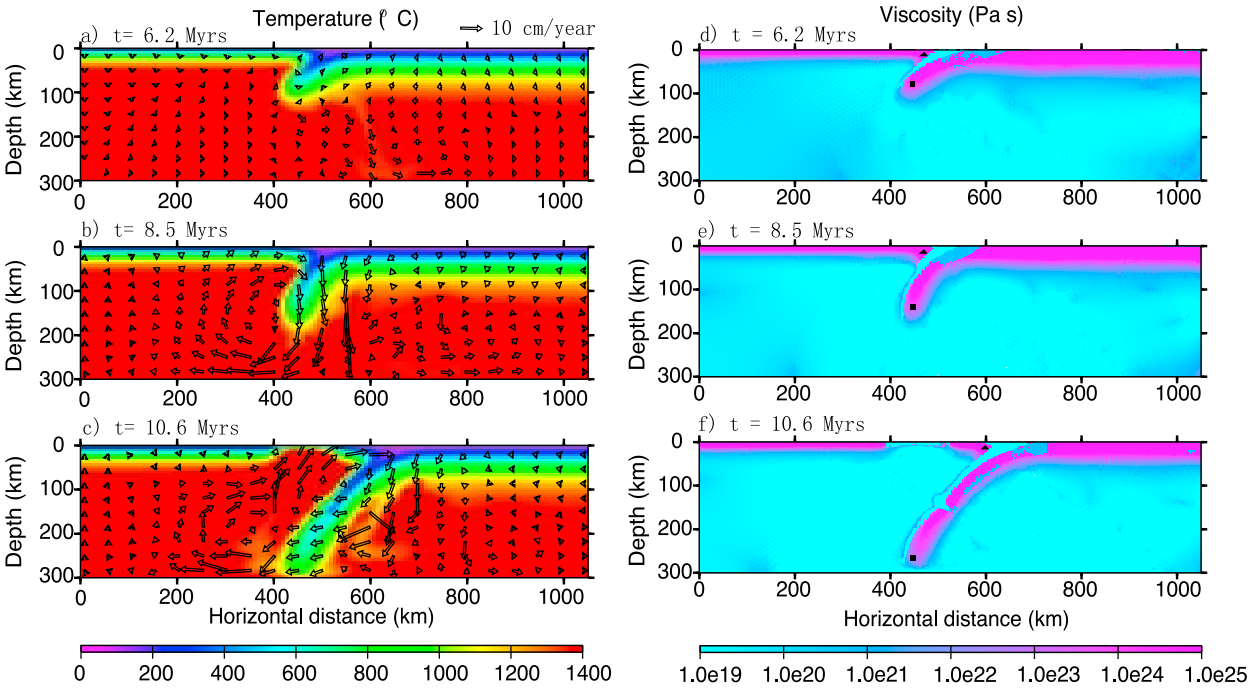

Figure 3. The temperature, velocity, and viscosity for case SI26 (continuous initiation with backarc spreading mode) at three different times: (a, d) at 6.2 Myrs, (b, e) at 8.5 Myrs, and (c, f) at 10.6 Myrs. The black square and triangle in viscosity field show the position of the sampling points in the subducting and overriding plate, respectively.

portion of the old plate cannot sustain the large stress and is stretched into a thin filament (Figures 5a and 5b). After the descent of the first segment of the old plate, continuous convergence leads to the bending and descent of another segment of the plate similar to the first one (Figure 5c). We also observe strong asthenospheric upwelling and backarc spreading within the young overriding plate (Figures 5b and 5c).

[17] When the strength of the plate increases with μ_0 and ε_f set to 0.6 and 0.4 (case SI64), respectively, we find a mode of continuous initiation without backarc spreading. Subduction initiation becomes more difficult to induce because a large negative buoyancy is required for bending the strong plate. Initiation starts after a longer time (t_i = 10.0 Myrs), or a cumulative convergence of 200 km. However, in contrast to the earlier models, the velocity of the subducting plate only slightly exceeds the imposed velocity (Figure 4b). We find no abrupt velocity increase, in contrast to the other two modes. The vertical velocity of the subducting plate continuously increases such that it becomes slightly larger than 2.0 cm/year and then decreases as the subducting plate approaches the bottom of the box (Figure 4b). The old plate quickly bends due to negative buoyancy at t_i = 10.0 Myrs. However, the yielding region of the old plate is limited (Figure 5d). Upwelling of asthenosphere occurs with subduction initiation, but the upwelling velocity is small (several cm/year) with no backarc spreading (Figure 5d).

[18] As μ_0 is varied between 0.0 to 0.6 and ε_f is varied between 0.05 and 0.5, we obtain the initiation time, t_i, backarc spreading time, t_b, and modes of subduction initiation for all 26 cases (Table 2 and Figures 6a and 6b). For all these cases, C_0 and C_f are 44 MPa and 4.4 MPa, respectively. Several conclusions can be inferred from this summary. First, the initiation time, t_i, increases with both μ_0 and ε_f (Table 2 and Figure 6a). For the parameter range explored, t_i varies significantly from less than 1 Myrs to 11 Myrs, representing ~20 to ~220 km of plate convergence. Second, as μ_0 and ε_f increase, the mode changes from segmented to continuous with backarc spreading, and eventually to continuous without backarc spreading (Figure 6a). If we further increase both μ_0 and ε_f to be larger than the range we currently explored, due to our limited box size, the vertical velocity of the subducting plate cannot exceed the velocity imposed to push the plate before the subducting plate slows through interaction with the bottom boundary, therefore no subduction initiation is observed. Third, backarc

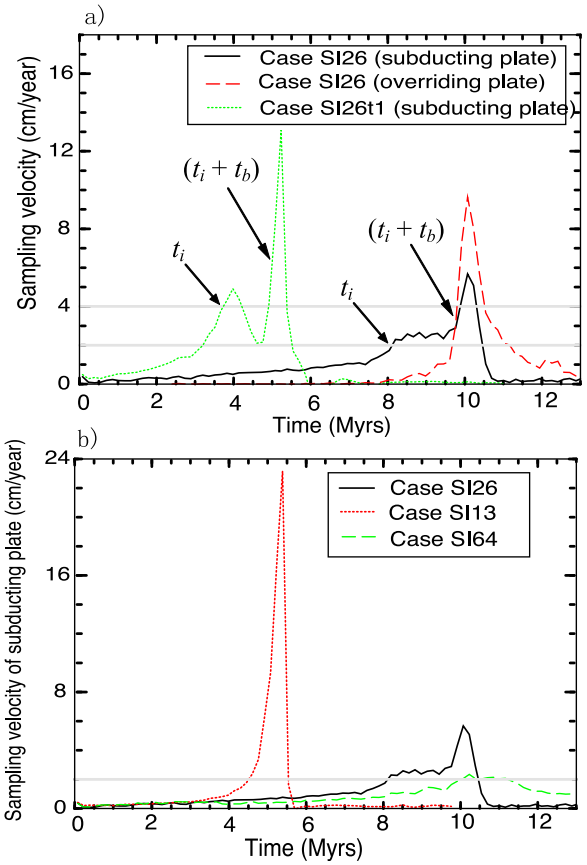

Figure 4. (a) The velocity of the sampling point in the subducting plate and in the overriding plate versus time for cases SI26. Solid line shows the vertical velocity of the subducting plate; Dashed line shows the horizontal velocity of the overriding plate. Dotted line shows the vertical velocity of the subducting plate for case SI26t1. Case SI26t1 is the same as SI26 except that the imposed velocity is doubled to 4 cm/year. The horizontal gray lines are at 2 and 4 cm/yr. (b) The vertical velocity of the sampling point in the subducting plate for cases SI26, SI13, SI64 which all have imposed velocity boundary condition. The horizontal gray line is the imposed velocity of 2 cm/year. The subduction initiation time, t_i, and the time when the backarc spreading starts, $t_i + t_b$, are marked for both cases.

spreading is not confined to the segmented mode. For some cases with the segmented mode, ε_f is relatively large and the descent of the old plate induces neither strong asthenospheric upwellings nor backarc spreading (Figure 6b, black circles).

[19] We test the effect of grid resolution on our model results. For case SI26, we increased the grid resolution from 128 × 64 to 160 × 80 elements to obtain case SI26h (Table 2), but kept the number of particles in each element at 16. The times of subduction initiation and backarc spreading are only slightly smaller compared with case SI26 (Table 2), indicating that our current resolution is sufficiently high to resolve the processes.

3.2. Role of Plate Age

[20] The influence of the age of subducting plate on subduction initiation has been studied. The aging of plates may facilitate subduction initiation by providing more negative buoyancy as the driving force, but may not necessarily provide more favorable conditions for initiating subduction due to the increased resistance to plate bending [*Cloetingh et al.*, 1989]. Here we use numerical cases to study the effects of subducting plate age on the mode of subduction initiation.

[21] For four cases (cases SI23, SI32, SI43 and SI51), where μ_0 equals ε_f in each case, the initiation mode changes from the segmented to continuous with backarc spreading, then to continuous without backarc spreading due to the increase of μ_0 and ε_f (Figure 6a). For these cases, we keep the age of the overriding plate at 2 Ma, and vary the age of the subducting plate between 12 and 82 Ma, while it was previously a constant 42 Ma. The corresponding subduction initiation time and mode show that as the subducting plate becomes younger, there is a trend for the mode to change from segmented to continuous with backarc spreading, and then to continuous without backarc spreading (Table 3 and Figure 7a). Case SI51c is represented by a black symbol in Figure 7a because the vertical velocity of the subducting plate does not exceed the imposed velocity before the subducting plate is resisted by the bottom boundary, thus no subduction initiation occurs. For a fixed subducting plate age, the subduction initiation time increases with increased μ_0 and ε_f (Figure 7a). However, the subduction initiation time does not monotonically decrease with plate age for fixed μ_0 and ε_f (Figure 7a and Table 3). This may reflect the competing effects of increased buoyancy of the old plate and increased resistance from plate bending. For those cases with backarc spreading, the backarc spreading time generally increases with decreased subducting plate age (Figure 7b).

3.3. Role of an Imposed Stress Boundary Condition

[22] For all the above cases, we consider that subduction initiation is driven by an imposed constant velocity boundary condition. It is also possible that subduction initiation is induced by an imposed

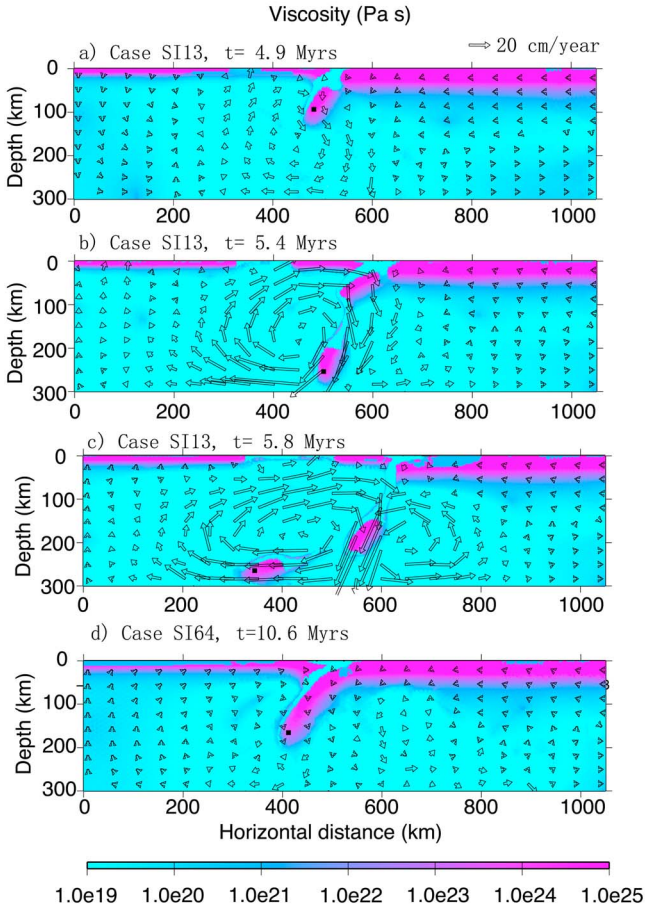

Figure 5. The viscosity structure overlain by velocity vectors. (a–c) For case SI13 at 4.9, 5.4 and 5.8 Myrs (the segmented initiation mode); (d) for case SI64 at 10.6 Myrs (the continuous initiation without backarc spreading mode). The black square in each frame shows the position of the sampling point in the subducting plate.

constant stress within the plate [e.g., *Toth and Gurnis*, 1998]. We test the effects of an imposed constant stress boundary condition (Figure 1b) on the mode of subduction initiation. In case SI26s1, otherwise identical to SI26, we change the boundary condition to be an imposed constant stress of 80 MPa applied down to 50 km depth (Figure 1b), which represents a tectonic force of 4×10^{12} N/m, approximately equal to the ridge push force for old oceanic lithosphere [*McKenzie*, 1977; *Turcotte and Schubert*, 2002]. With this boundary condition, subducting plate velocity at the sampling point increases significantly to tens of cm/year within 1 Myrs (Figure 8), and the subducting plate reaches the bottom of the box by 1.4 Myrs (Figure 9a). In contrast to the otherwise identical case with an imposed velocity (SI26), here the subducting plate does not founder throughout the whole initiation process. As a result, there is neither trench retreat nor backarc spreading for case SI26s1 (Figure 9a). We change the magnitude of the imposed stress from 80 MPa to 120 MPa and 60 MPa for cases SI26s2 and SI26s3, respectively. The time for the subducting plate to reach the bottom of the box increases with a decreased value of imposed stress (Figure 8). If we further reduce the stress to 40 MPa, which is smaller than the initial cohesion of the plate, no subduction initiation is observed. For case SI26s4, we fix the position of the plate interface while increasing the box size from 1050 km to 1400 km such that the length of the subducting plate is increased from ~500 km to ~800 km. The time for the subducting plate to reach the bottom of the box slightly increases to ~2.0 Myrs (Figures 8 and 9b), indicating the effects of the increased resistant force due to viscous shear from asthenosphere beneath the plate. We do not observe foundering of the subducting plate and backarc spreading for cases SI26s1 through SI26s4, and conclude that an imposed stress boundary condition does not favor the occurrence of backarc spreading compared to an imposed velocity boundary

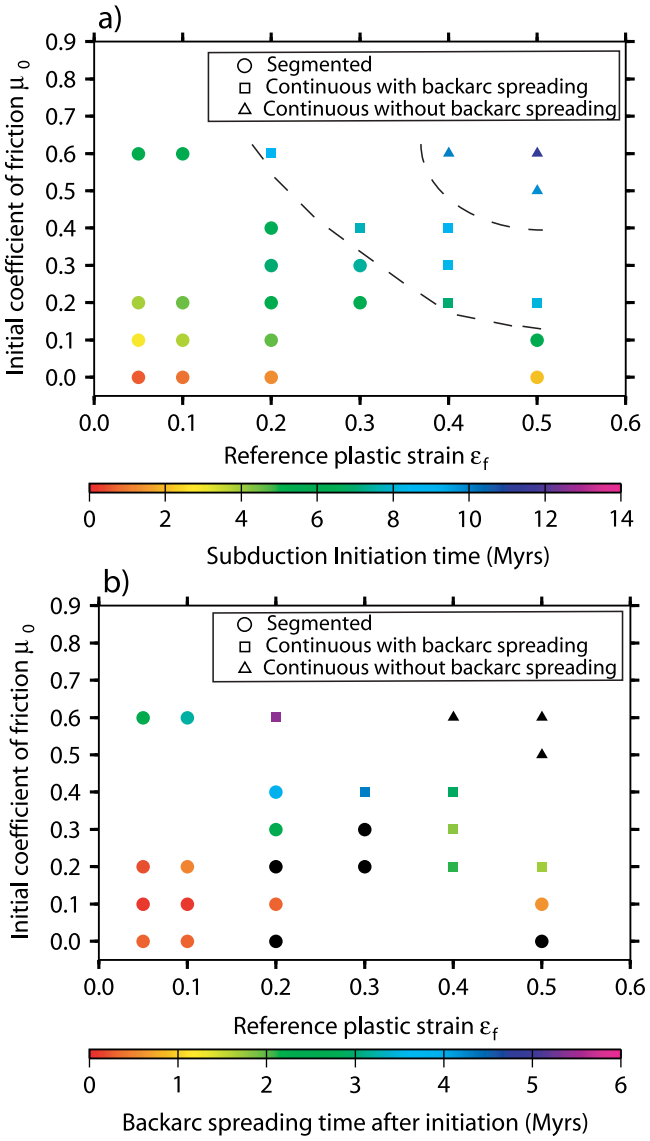

Figure 6. (a) Our classified modes of subduction initiation versus initial coefficient of friction, μ_0, and reference plastic strain, ε_f. The dashed lines show the boundaries between different modes. The color code shows the subduction initiation time. (b) Backarc spreading time, i.e., time interval between subduction initiation time and the time when backarc spreading starts, for cases with different initial coefficient of friction, μ_0, and reference plastic strain, ε_f. Black symbols represent cases with no backarc spreading.

condition. An imposed velocity boundary condition prevents the subducting plate from exceeding the imposed velocity value with the addition of slab pull [*Toth and Gurnis*, 1998], thus promotes plate foundering, trench retreat and backarc spreading.

3.4. Sensitivity Test for the Nominal Values

[23] With SI26 as a reference case, we test the effects of model parameters which had been held constant. We show that the variations of the magnitude of imposed velocity, the initial cohesion of the plates, and the depth of the box from their nominal values do not affect the mode of subduction initiation, but have small effects on the subduction initiation time and backarc spreading time.

[24] We first test the effects of the magnitude of the imposed velocity on the subduction initiation mode. Case SI26t1 is identical to case SI26 (Table 3), except that the imposed velocity at the right boundary of the plate is doubled (to 4 cm/year). We obtain the same subduction initiation mode of continuous with backarc spreading, however, with the doubling of imposed velocity, the

Table 3. Cases With Different Subducting Plate Ages, Different Boundary Condition and Different Model Nominal Values, and Resulted Modes of Subduction Initiation[a]

Case	μ_0	ε_f	Plate Age (Ma)	t_i (Myrs)	t_b (Myrs)	Modes
SI23	0.2	0.2	42	5.3	-	S
SI23b	0.2	0.2	12	7.1	-	S
SI23c	0.2	0.2	22	5.6	-	S
SI23d	0.2	0.2	82	5.3	0.1	S
SI32	0.3	0.3	42	7.4	-	S
SI32b	0.3	0.3	12	10.4	4.7	CB
SI32c	0.3	0.3	22	11.7	0.7	CB
SI32d	0.3	0.3	82	9.3	0.3	S
SI43	0.4	0.4	42	8.9	2.9	CB
SI43b	0.4	0.4	12	10.5	-	C
SI43c	0.4	0.4	22	13.7	-	C
SI43d	0.4	0.4	82	10.0	0.3	CB
SI51	0.5	0.5	42	9.8	-	C
SI51b	0.5	0.5	12	10.5	-	C
SI51c	0.5	0.5	22	-	-	-
SI51d	0.5	0.5	82	11.4	0.6	CB
SI26s1	0.4	0.4	42	-	-	C
SI26s2	0.4	0.4	42	-	-	C
SI26s3	0.4	0.4	42	-	-	C
SI26s4	0.4	0.4	42	-	-	C
SI26t1	0.2	0.5	42	3.7	1.5	CB
SI26t2	0.2	0.5	42	7.4	0.8	CB
SI26t3	0.2	0.5	42	8.4	2.9	CB
SI26t4	0.2	0.5	42	5.1	1.2	CB

[a]Similar to Table 2, except that we add a column, "Plate age," to indicate the different ages of the subducting plate. For case SI51c, the velocity of the sampling points cannot exceed the imposed velocity before the plate is resisted by the bottom boundary. For case SI26s1 to SI26s4, the subduction initiation time is not defined because they use an imposed constant stress boundary condition.

subduction initiation time is approximately halved (Figure 4a), indicating that the time for subduction initiation is controlled by the total amount of convergence, as earlier found by *Hall et al.* [2003]. After the subduction initiation starts, backarc spreading time is not strongly related to the imposed velocity (Table 3 and Figure 4a).

[25] We then test the effects of the initial cohesion, C_0, which controls plate strength when no plastic strain is accumulated. The initial cohesion is set to 20 MPa and 60 MPa for case SI26t2 and SI26t3, respectively (C_0 is 44 MPa for all other cases). The results show that it does not affect the subduction initiation mode (Table 3). But both subduction initiation time and time to the onset of backarc spreading moderately increase with increased initial cohesion of the plates while the times decrease with the decreased cohesion (Table 3).

[26] Last, we extend the box depth from 350 km to 450 km from case SI26t4, while keeping the air layer thickness at 50 km. The subduction initiation time, 5.1 Myrs, and backarc spreading time, 1.2 Myrs, are both reduced compared with case SI26, suggesting that a deeper box facilitates the initiation of subduction. In case SI26t4, the whole region beneath the lithosphere has a low viscosity. We do not increase viscosity with depth. As a result, a deeper box promotes stronger asthenospheric flow and facilitates subduction initiation. Considering that the low viscosity zone beneath the lithosphere probably only extends to 200–300 km depth for the Earth's mantle [*Mitrovica and Peltier*, 1993; *Karato*, 2010], a box with a depth of 350 km (300 km excluding the air layer) used in this study is more reasonable for subduction initiation modeling. Nevertheless, it is worthwhile for future work to study subduction initiation with a more realistic model that includes the whole upper mantle with a depth-dependent viscosity profile.

4. Discussion

[27] Previously, all known subduction initiation events (essentially, examples from the Pacific since 50 Ma) were placed in the context of a single evolutionary pathway in which tectonics of the system at any time reflected a progression of an evolving force balance [*Gurnis et al.*, 2004]. The sequence is composed of initial trench formation due to plate compression, foundering of the slab, rapid trench rollback and backarc spreading. Our expanded model study confirms this evolution pathway (continuous subduction with backarc spreading), but we have discovered that this pathway is not unique. Different plastic parameters and subducting plate age may lead to two additional pathways: the segmented and continuous without backarc spreading.

[28] The segmented initiation mode may be generated with continuous convergence between two adjacent plates. This mode is different from a classical mode of subduction. First, it is not self-sustaining because the negative buoyancy of slab overcomes the strength of the lithosphere and small segments continually tear off from the slab. Second, the tearing may produce little or no extensional deformation in the overriding plate. The New Hebrides subduction zone probably initiated with this mode. The New Hebrides subduction zone initiated through a polarity reversal at ~10–12 Ma [*Greene et al.*, 1994]. Here, a slab segment beneath the North Fiji Basin is characterized by an unusual group of more than 100 earthquakes located at ~600 km depth [*Hamburger and Isacks*, 1987; *Okal and Kirby*, 1998; *Richards et al.*, 2011]. This detached slab segment may have broken

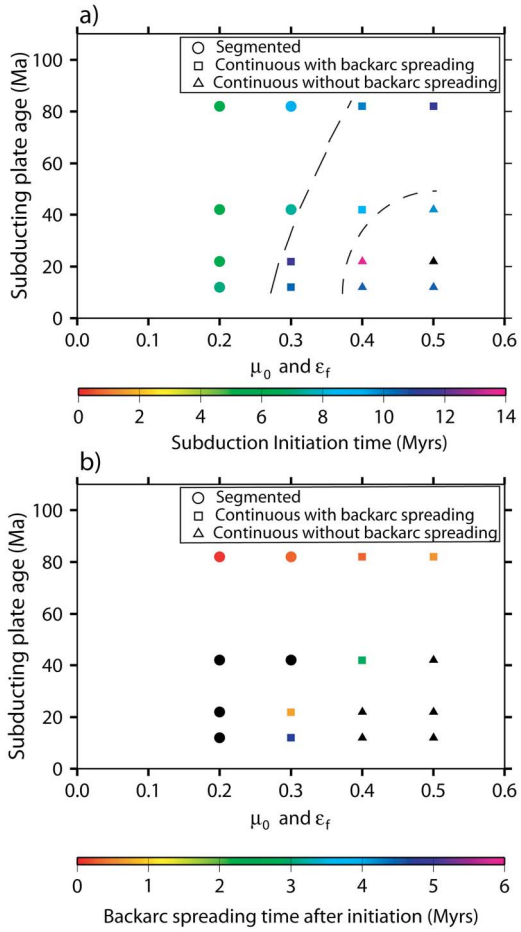

Figure 7. (a) The effect of the age of the subducting plate on the different modes of subduction initiation. The dashed lines show the boundaries between different modes. The color code shows the subduction initiation time. Notice that the black triangle in Figure 7a indicates that for case SI51c, the velocity of the sampling point in the subducting plate cannot exceed the imposed velocity before the subducting plate is resisted by the bottom boundary. (b) Backarc spreading time for cases with different subducting plate ages. Black symbols represent cases with no backarc spreading.

off the subducted Australian plate at ~5 Ma ago according to the structural interpretation of *Richards et al.* [2011]. Consequently, the segmentation would have occurred ~5–7 Myrs after subduction initiation of the Australian plate. The New Hebrides trench has been consuming Australian plate which is continuous with the crust of the South Fiji Basin. Therefore, such subducted crust is rather young and would have been formed within a backarc basin [*Seton et al.*, 2010]. Through the formation of oceanic crust within a backarc, it is possible that the crust is more volatile rich and mechanically weak. We speculate that if the crust is weak it would lie within the segmented mode (Figure 10a).

[29] Continuous initiation without backarc spreading is accompanied by a slow increase of velocity of the downgoing slab and relatively weak asthenospheric upwelling. In this mode, the lack of backarc spreading would imply little arc volcanism. This may explain why we sometimes fail to observe volcanism for places where subduction initiation has been known to occur. For example, the Puysegur subduction zone, i.e., the northern segment of the Macquarie Ridge Complex between the Australian and Pacific plates, has undergone convergence since ~15 Ma. Although the downdip tip of the slab has reached 150 km depth [*Sutherland et al.*, 2009], only small isolated sea mounts are known on the Pacific plate, most notably Solander Island. In addition, no backarc spreading is observed on the overriding Pacific plate either where the Australian plate subducts beneath oceanic crust along the Puysegur Ridge or below continental crust in the Fiordland region of New Zealand's South Island. The subducting plate age for the Puysegur zone is also young, ~30 Ma [*Seton et al.*, 2010]. Therefore, if the subducting plate strength is relatively strong, then this would allow the subduction initiation to fall within the mode of continuous without backarc spreading (Figure 10a).

[30] The effects of boundary conditions, including imposed velocity and stress, may explain the different initiation history inferred between IBM and the Aleutian subduction zone. The IBM subduction zone may have been induced obliquely along the strike of the western boundaries of the Pacific plate [e.g., *Seton et al.*, 2010]. The voluminous eruption of boninites in the IBM subduction zone [*Stern and Bloomer*, 1992; *Reagan et al.*, 2010; *Ishizuka et al.*, 2011] provides the type example of continuous initiation with backarc spreading. Because the large Pacific plate moved at a rate dictated by all of the subduction forces around its edge as well as ridge push from the distal Pacific-Farallon spreading center, IBM initiation can be largely viewed as induced by an imposed constant velocity (Figure 10b). After sufficient convergence, the subducting plate bends and founders. Due to the regulation of the Pacific plate by all of the forces, the Pacific plate does not substantially increase its velocity. Consequently, trench retreat and backarc spreading are induced in response to slab foundering (Figure 10b). In contrast to the large Pacific plate that existed when the IBM initiated, the Kula plate that subducted along the Aleutian during its phase of initiation was a

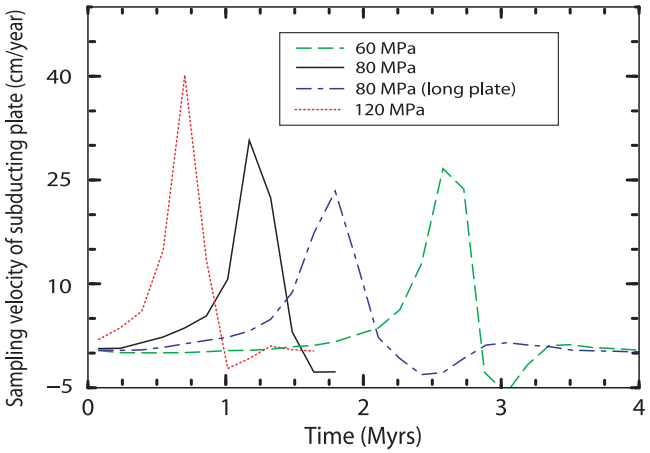

Figure 8. The vertical velocity of the sampling point in the subducting plate versus time for cases with imposed stress boundary condition: SI26s1 (80 MPa), SI26s2 (120 MPa), SI26s3 (60 MPa), and SI26s4 (80 MPa and long plate).

much smaller, confined plate. Indeed, the Kula-Pacific ridge was just a few thousand kilometers away from the nascent trench [*Seton et al.*, 2010]. When subduction ceased along the Bering Sea Alaskan margin [e.g., *Seton et al.*, 2010], subduction likely initiated along the present Aleutian chain at ~46 Ma [*Jicha et al.*, 2006]. A constant stress boundary condition within the oceanic plate is a reasonable model to apply to the Kula/Aleutian subduction initiation system. The constant stress condition would be akin to the force from the single ridge system along the southern Kula-Pacific ridge of this small plate. An imposed constant stress in the mechanical models leads to no intense asthenospheric upwelling (and by implication no boninites) and backarc spreading which is the observed outcome of Aleutian initiation (Figure 10b).

[31] Previous studies predict catastrophic subduction initiation after about 100 km of convergence [*Hall et al.*, 2003]. Compared with the results here, the amount of convergence does not appear to be a constant, but depends on plate strength, especially the initial coefficient of friction and reference plastic strain which were mostly fixed in previous studies. *Hall et al.* [2003] considered the effects of pore pressure on the yield stress of the lithosphere, such that their initial coefficient of friction is only

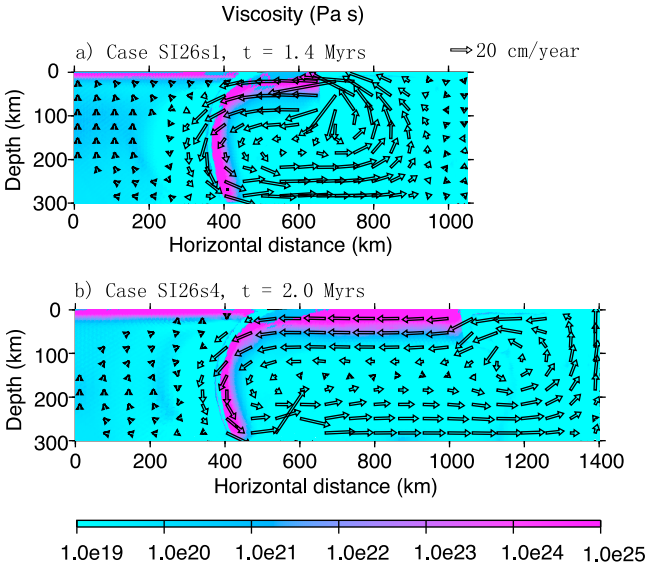

Figure 9. The viscosity structure and velocity vectors for cases with imposed stress boundary condition. (a) For case SI26s1 at 1.4 Myrs; (b) for case SI26s4 at 2.0 Myrs. The black square in each frame shows the position of the sampling point in the subducting plate.

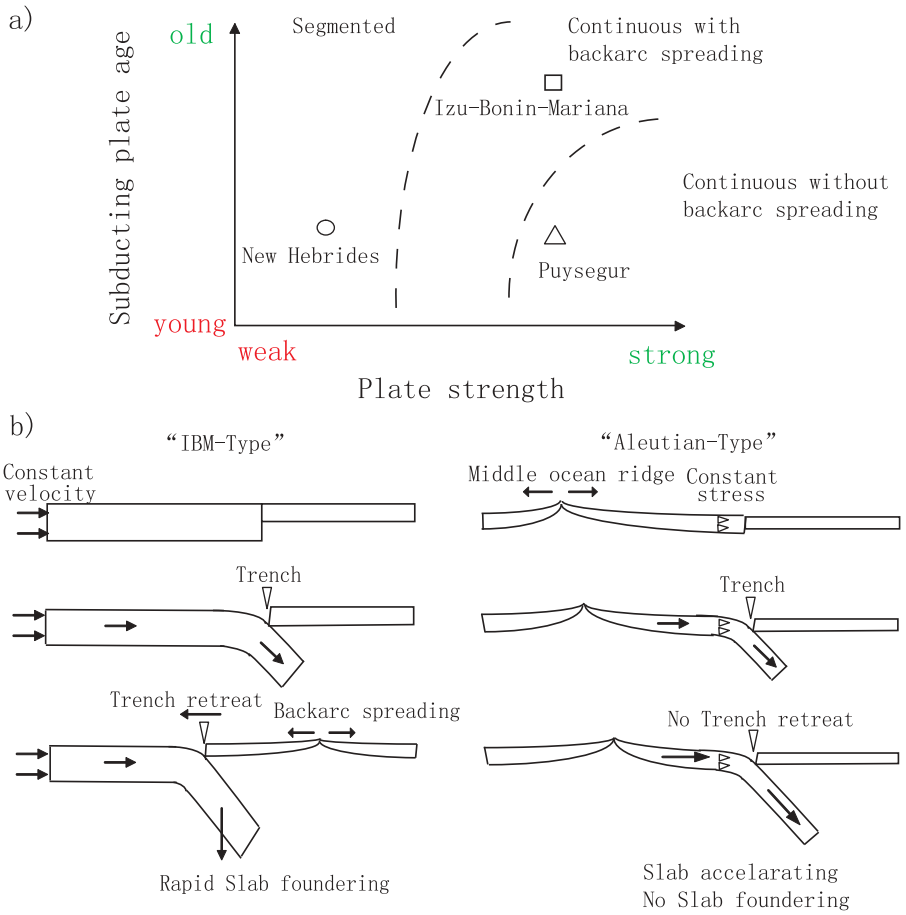

Figure 10. (a) Conceptualization of our suggested plate strength, subducting plate age, and subduction initiation modes for the New Hebrides, Izu-Bonin-Mariana and Puysegur subduction zones. (b) The different subduction initiation modes result from different large-scale force settings for the IBM and Aleutian subduction zones. We hypothesize that an imposed velocity regulated IBM initiation by all of the forces around the large Pacific plate such that the subduction zone foundered with extensive backarc spreading. On the other hand, when the Aleutian subduction zone formed, the constant ridge-push forces could regulate the Kula plate such that there was no plate foundering and the Aleutian trench did not rapidly rollback.

slightly larger than 0 and smaller then 0.1. From our results, this small coefficient of friction leads to a segmented mode of subduction initiation (Figure 6a). Therefore, we suspect that the catastrophic subduction initiation observed by *Hall et al.* [2003] may actually be the starting stage of the segmented mode of subduction initiation. Possibly because of the difference in numerical method, (*Hall et al.* [2003] used an explicit method while an implicit method is used here), the segmented mode was not earlier observed.

[32] Our results provide a first order understanding for the effects of plastic parameters on the mode of subduction initiation. The mantle material properties are set to be homogeneous except in a small weak zone. However, overriding and subducting plates are heterogeneous. The involvement of crust, the variation in the chemical composition of the subducting and the overriding plates, phase transitions and dehydration of the slab all alter the properties of plates. For example, the formation of serpentine may significantly reduce the mantle viscosity and induce subduction initiation [*Hilairet et al.*, 2007]. Therefore for specific tectonic setting, the evolutionary mode of subduction initiation needs to be compared against realistic simulations with heterogeneous plate properties. In the computations here, we did not consider the effects of shear heating which may affect the occurrence of shear localization and subduction initiation [*Thielmann and Kaus*, 2011]. However, without including shear heating, we still observe strong shear localization for all of our cases under continuous convergence (e.g., Figure 2c). It is worth noting that our 2-D model results can be applied to subduction

initiation for slabs with a long along-strike dimension. However, for narrow slabs, 3-D effect (e.g., flow around the slab) may be important and could affect the details of subduction initiation. A full 3-D model is therefore necessary to obtain more comprehensive understanding of subduction initiation.

5. Conclusion

[33] In conclusion, we explored the effects of plastic parameters and subducting plate age on the evolutionary mode of induced subduction initiation with a visco-elasto-plastic geodynamic model. With imposed velocity boundary conditions, we find three evolutionary pathways of subduction initiation: segmented, continuous with backarc spreading and continuous without backarc spreading. With an increase in the coefficient of friction and reference plastic strain, the mode gradually changes from segmented to continuous with backarc spreading and eventually to continuous without backarc spreading. The amount of convergence needed for subduction initiation significantly increases from ~20 to ~220 km. The same transition of evolutionary mode is observed when the age of subducting plate becomes younger. If the imposed velocity boundary condition is changed to an imposed constant stress in the plate, the amount of convergence needed for subduction initiation is significantly reduced and backarc spreading is not observed.

[34] These geodynamic models provide a basis for understanding the cause for the observed divergent geological pathways of subduction initiation including the IBM and Aleutians as well as other subduction zones that have initiated more recently. The segmented mode of subduction initiation is different from a classical subduction process. It is not self-sustaining because the negative buoyancy forces of the slab overcome the strength of the lithosphere and small plate segments continually tear off from the slab. The tearing of the plate segments may produce little or no extensional deformation in the overriding plate. This mode may explain the formation of the New Hebrides subduction zone where a segmented slab is found in the upper mantle. This slab segment probably tore off from the subducting plate shortly after subduction initiated. The mode of continuous with backarc spreading is a favorable explanation for the well developed IBM subduction system where strong backarc spreading and voluminous boninite eruption followed initiation. In contrast, the mode of continuous subduction initiation without backarc spreading may provide explanations for the scarce distribution of arc volcanism in Puysegur subduction zone where the convergence between the Australia and Pacific plates has been under way since 15 Ma.

Acknowledgments

[35] This work was supported by the National Science Foundation (NSF EAR-0810303) and the Gordon and Betty Moore Foundation through the Caltech Tectonics Observatory. This is contribution 179 of the Caltech Tectonics Observatory. We thank Satoru Honda for a helpful review of the manuscript.

References

Buck, W. R., and A. N. B. Poliakov (1998), Abyssal hills formed by stretching oceanic lithosphere, *Nature*, *392*, 272–275, doi:10.1038/32636.

Byerlee, J. (1978), Friction of rocks, *Pure Appl. Geophys.*, *116*, 615–626, doi:10.1007/BF00876528.

Cloetingh, S., R. Wortel, and N. J. Vlaar (1989), On the initiation of subduction zones, *Pure Appl. Geophys.*, *129*, 7–25, doi:10.1007/BF00874622.

Crameri, F., P. Tackley, I. Meilick, T. Gerya, and B. Kaus (2011), A free plate surface and weak oceanic crust produce single-sided subduction on Earth, paper presented at 12th International Workshop on Modeling of Mantle Convection and Lithosphere Dynamics, Eur. Geosci. Union, Dollnsee, Germany.

Greene, H. G., J. Y. Collot, M. A. Fisher, and A. J. Crawford (1994), Neogene tectonic evolution of the New Hebrides island arc: A review incorporating ODP drilling results, *Proc. Ocean Drill. Program Sci. Results*, *134*, 19–46.

Gurnis, M., C. Hall, and L. Lavier (2004), Evolving force balance during incipient subduction, *Geochem. Geophys. Geosyst.*, *5*, Q07001, doi:10.1029/2003GC000681.

Hall, C. E., M. Gurnis, M. Sdrolias, L. L. Lavier, and R. D. Muller (2003), Catastrophic initiation of subduction following forced convergence across fracture zones, *Earth Planet. Sci. Lett.*, *212*, 15–30, doi:10.1016/S0012-821X(03)00242-5.

Hamburger, M. W., and B. L. Isacks (1987), Deep earthquakes in the southwest Pacific: A tectonic interpretation, *J. Geophys. Res.*, *92*, 13,841–13,854, doi:10.1029/JB092iB13p13841.

Hilairet, N., B. Reynard, Y. B. Wang, I. Daniel, S. Merkel, N. Nishiyama, and S. Petitgirard (2007), High-pressure creep of serpentine, interseismic deformation and initiation of subduction, *Science*, *318*, 1910–1913, doi:10.1126/science.1148494.

House, M. A., M. Gurnis, P. J. J. Kamp, and R. Sutherland (2002), Uplift in the Fiordland region, New Zealand: Implications for incipient subduction, *Science*, *297*, 2038–2041, doi:10.1126/science.1075328.

Hughes, T. J. R. (2000), *The Finite Element Method: Linear Static and Dynamic Finite Element Analysis*, 682 pp., Dover, Mineola, N. Y.

Ishizuka, O., et al. (2011), The timescales of subduction initiation and subsequent evolution of an oceanic island arc, *Earth Planet. Sci. Lett.*, *306*, 229–240, doi:10.1016/j.epsl.2011.04.006.

Jicha, B. R., D. W. Scholl, B. S. Singer, G. M. Yogodzinski, and S. M. Kay (2006), Revised age of Aleutian island arc formation implies high rate of magma production, *Geology*, *34*, 661–664, doi:10.1130/G22433.1.

Karato, S. I. (2010), Rheology of the Earth's mantle: A historical review, *Gondwana Res.*, *18*, 17–45, doi:10.1016/j.gr.2010.03.004.

Karato, S. I., and P. Wu (1993), Rheology of the upper mantle: A synthesis, *Science*, *260*, 771–778, doi:10.1126/science.260.5109.771.

McKenzie, D. P. (1977), The initiation of trenches: A finite amplitude instability, in *Island Arcs, Deep Sea Trenches, and Back-Arc Basins*, *Maurice Ewing Ser.*, vol. 1, edited by M. Talwani and W. C. Pitman III, pp. 57–61, AGU, Washington, D. C.

Mitrovica, J. X., and W. R. Peltier (1993), The inference of mantle viscosity from an inversion of the Fennoscandian relaxation spectrum, *Geophys. J. Int.*, *114*, 45–62, doi:10.1111/j.1365-246X.1993.tb01465.x.

Moresi, L., S. J. Zhong, and M. Gurnis (1996), The accuracy of finite element solutions of Stokes' flow with strongly varying viscosity, *Phys. Earth Planet. Inter.*, *97*, 83–94, doi:10.1016/0031-9201(96)03163-9.

Moresi, L., F. Dufour, and H. B. Muhlhaus (2003), A Lagrangian integration point finite element method for large deformation modeling of viscoelastic geomaterials, *J. Comput. Phys.*, *184*, 476–497, doi:10.1016/S0021-9991(02)00031-1.

Mueller, S., and R. J. Phillips (1991), On the initiation of subduction, *J. Geophys. Res.*, *96*, 651–665, doi:10.1029/90JB02237.

Nikolaeva, K., T. V. Gerya, and F. O. Marques (2010), Subduction initiation at passive margins: Numerical modeling, *J. Geophys. Res.*, *115*, B03406, doi:10.1029/2009JB006549.

Niu, Y., M. J. O'Hara, and J. A. Pearce (2003), Initiation of subduction zones as a consequence of lateral compositional buoyancy contrast within the lithosphere: A petrological perspective, *J. Petrol.*, *44*, 851–866, doi:10.1093/petrology/44.5.851.

Okal, E. A., and S. H. Kirby (1998), Deep earthquakes beneath the Fiji Basin, SW Pacific: Earth's most intense deep seismicity in stagnant slabs, *Phys. Earth Planet. Inter.*, *109*, 25–63, doi:10.1016/S0031-9201(98)00116-2.

Poliakov, A. N. B., and W. R. Buck (1998), Mechanics of stretching elastic-plastic-viscous layers: Applications to slow-spreading mid-ocean ridges, in *Faulting and Magmatism at Mid-Ocean Ridges*, *Geophys. Monogr. Ser.*, vol. 106, edited by W. R. Buck, et al., pp. 305–323, AGU, Washington, D. C., doi:10.1029/GM106p0305.

Reagan, M. K., et al. (2010), Fore-arc basalts and subduction initiation in the Izu-Bonin-Mariana system, *Geochem. Geophys. Geosyst.*, *11*, Q03X12, doi:10.1029/2009GC002871.

Richards, S., R. Holm, and G. Barber (2011), When slabs collide: A tectonic assessment of deep earthquakes in the Tonga-Vanuatu region, *Geology*, *39*, 787–790, doi:10.1130/G31937.1.

Seton, M., R. D. Muller, and C. Gaina (2010), Reconstructing the early Jurassic to present Pacific and proto-Pacific Basins: Implications for circum-Pacific plate margins, paper presented at Australian Earth Sciences Convention, Geol. Soc. Aust., Canberra, July.

Stern, R. J. (2004), Subduction initiation: Spontaneous and induced, *Earth Planet. Sci. Lett.*, *226*, 275–292.

Stern, R. J., and S. H. Bloomer (1992), Subduction zone infancy: Examples from the Eocene Izu-Bonin-Mariana and Jurassic California arcs, *Geol. Soc. Am. Bull.*, *104*, 1621–1636, doi:10.1130/0016-7606(1992)104<1621:SZIEFT>2.3.CO;2.

Sutherland, R., F. Davey, and J. Beavan (2000), Plate boundary deformation in South Island, New Zealand, is related to inherited lithosphere structure, *Earth Planet. Sci. Lett.*, *177*, 141–151, doi:10.1016/S0012-821X(00)00043-1.

Sutherland, R., M. Gurnis, P. J. J. Kamp, and M. A. House (2009), Regional exhumation history of brittle crust during subduction initiation, Fiordland, southwest New Zealand, and implications for thermochronologic sampling and analysis strategies, *Geosphere*, *5*, 409–425, doi:10.1130/GES00225.1.

Sutherland, R., et al. (2010), Lithosphere delamination with foundering of lower crust and mantle caused permanent subsidence of New Caledonia Trough and transient uplift of Lord Howe Rise during Eocene and Oligocene initiation of Tonga-Kermadec subduction, western Pacific, *Tectonics*, *29*, TC2004, doi:10.1029/2009TC002476.

Thielmann, M., and B. J. P. Kaus (2011), Shear heating and subduction initiation, paper presented at 12th International Workshop on Modeling of Mantle Convection and Lithosphere Dynamics, Eur. Geosci. Union, Dollnsee, Germany.

Toth, J., and M. Gurnis (1998), Dynamics of subduction initiation at pre-existing fault zones, *J. Geophys. Res.*, *103*, 18,053–18,067, doi:10.1029/98JB01076.

Turcotte, D. L., and G. Schubert (2002), *Geodynamics*, 2nd ed., 456 pp., Cambridge Univ. Press, New York.